Observation of Polarization Singularities at Nanoscale

M. Burresi,[1,*] R. J. P. Engelen,[2] A. Opheij,[2] D. van Oosten,[2] D. Mori,[3] T. Baba,[3] and L. Kuipers[2]

[1] *Center for Nanophotonics, FOM Institute for Atomic and Molecular Physics (AMOLF), Kruislaan 407, 1098 SJ Amsterdam, The Netherlands Kruislaan 407 Amsterdam 1009 SJ Amsterdam, The Netherlands*

[2] *Center for Nanophotonics, FOM Institute for Atomic and Molecular Physics (AMOLF), Kruislaan 407, 1098 SJ Amsterdam, The Netherlands*

[3] *Yokohama National University, Departement of Electrical and Computer Engineering, 79-5 Tokiwadai, Hodogayaku, Yokohama 240-8501, Japan*

(Dated: August 1, 2008)

Using a phase-sensitive near-field microscope, we measure the in-plane electric vector field distribution of light propagating through a 2D photonic crystal waveguide with sub-wavelength resolution. We identify time-dependent and time-independent polarization singularities and investigate the topology of the surrounding electric field.

PACS numbers:

A wave singularity can be defined as a position in space where a property of a wave is not defined. Such singularities can be found in many types of wave and they can have a large impact on common life. For instance, they play an important role in heart fibrillation [1] or in the distribution of riptides [2]. Moreover, wave singularities are studied in many different fields of physics, such as high energy physics [3], Bose-Einstein condensate [4–6], superconductivity [7] and superfluidity [8]. In optics, wave singularities have been studied since the 1830s (for an overview, see for instance Berry [9]) and have been observed in the interference patterns of the diffracted light that is surrounding us. The simplest class of wave singularity is the so-called wave dislocation [10] (vortex, phase singularity, edge dislocation, etc.), which is a scalar field singularity that occurs where the amplitude of a complex valued field is zero [11, 12]. Another more subtle class is the so-called polarization singularity (C-points, L-lines and disclinations), which occurs in vector field on location where one of the parameters that define the polarization state is ill-defined [13–15]. In the last few years polarization singularities have been investigated in optics in the context of tightly focused beams [16], crystal optics [17], skylights [18] and speckle fields [19, 20]. Recently, the polarization state of light in photonic nanostructures has attracted particular interest in the nano-optics community. For instance, it has been suggested [21] that, exploiting the polarization state of an evanescent field at nanoscale, one could control the spin states in electronic micro-systems, polarization-sensitive chemical reactions and photon reactive molecules. Near-field microscopy has already proven to be a powerful tool in studies of the polarization distribution close to photonic nanostructures [22, 23]. In this work, we investigate the presence of polarization singularities in a 2D photonic crystal waveguide. We probe the evanescent field above the waveguide surface with a phase-sensitive near-field microscope [24–26] and reconstruct the distribution of the in-plane electric field components.

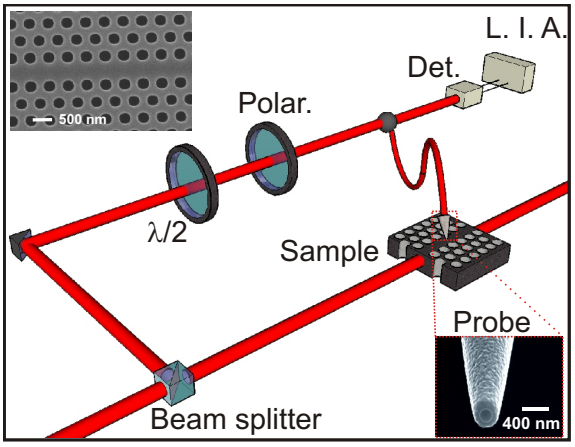

FIG. 1: (color) Schematic representation of the experimental setup. Light is coupled into a 2D photonic crystal waveguide. The near-field probe is scanned above the sample and collects the light that is subsequently interferometrically mixed with a reference beam and detected using a heterodyne scheme. The polarization state in the reference branch is controlled using waveplates. (left inset) Scanning electron micrograph of the silicon membrane photonic crystal waveguide under investigation (lattice constant $a = 450$ nm and hole diameter $d = 250$ nm). (right inset) Scanning electron micrograph of the aluminum-coated near-field probe with aperture of $\simeq 200$ nm.

The setup is schematically shown in Fig 1. The inset in the upper-left corner shows the photonic crystal waveguide used in this work. The sample consist of a silicon membrane with a thickness 200 nm and a periodic triangular arrangement of holes (lattice constant a=450 nm). The waveguide is formed by a single missing row of holes. The light source used to investigate the sample is a diode laser tuned to vacuum wavelength of 1463 nm. The light is coupled into the waveguide by focusing it on the entrance facet. The field above the sample is picked up by the sub-wavelength aperture of an aluminum-coated near-field probe [27] (lower-right inset

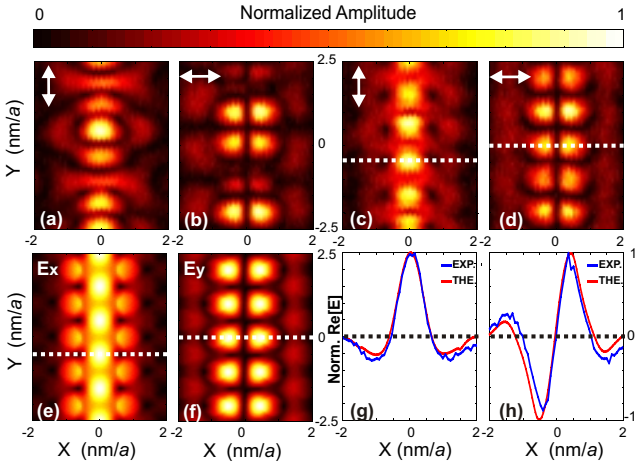

FIG. 2: (color)(a) and (b) Detected amplitude pattern for two orthogonal polarizations (indicated by white arrows) in the reference branch. (c) and (d) Amplitude pattern of the forward propagating mode, obtained after Fourier analysis of (a) and (b). (e) and (f) Theoretical amplitude pattern of E_x and E_y 20 nm above the surface for the forward propagating mode. For all the images the depicted area is $4a \times 5a$ (the center of the waveguide is at $x = 0$) and the amplitude is normalized. (g) and (h) Crosscuts of the experimentally (blue) and theoretically (red) obtained real part of the complex field along the dashed lines of (c), (d), (e) and (f), respectively.

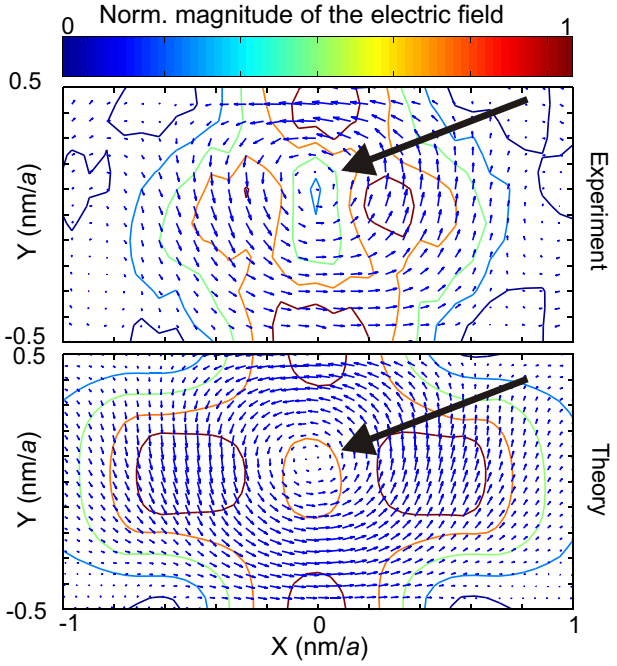

FIG. 3: (color) Experimentally and theoretically obtained instantaneous 2D vector plots of the electric field. The contour plots indicate the normalized magnitude of the electric field. The black arrows highlights a disclination. For both the figures the depicted area is $2a \times 1a$ (the center of the waveguide is at $x = 0$).

of Fig 1), that is kept 20 nm above the sample using shear force feedback. The light collected by the probe is interferometrically mixed with a reference signal and subsequently recorded using heterodyne detection [24–26]. Raster scanning the near-field probe above the 2D photonic structure, we recover the phase and the amplitude pattern of the light field in the photonic crystal waveguide with sub-wavelength resolution. When two orthogonal polarizations are present in the probe fiber, we can select one of the two by choosing the appropriate polarization for the reference branch.

Figs 2(a) and (b) show the amplitude pattern recorded for two orthogonal polarizations of the reference signal. The amplitude is normalized to the maximum value and the scanned area is $4a \times 5a$. The waveguide is centered around $x = 0$. Using Fourier analysis, we observe the presence of both forward and backward propagating Bloch modes in the photonic crystal waveguide [28]. We attribute the backward propagating mode to light that is reflected at the end-facet of the waveguide. When we select only the forward propagating mode by applying a Fourier filter to the experimental data [28], we obtain the amplitude distribution shown in Figs 2(c) and (d). Fig 2(e) and (f) show the amplitude of the E_x and E_y components of the electric field, respectively, of the forward propagating mode, as obtained using 3D finite-difference time-domain (FDTD) calculation. Figs 2(g) and (h) show the line traces of the real part of the complex signals along the dashed lines of Figs 2(c), (d), (e) and (f). Blue corresponds to the measurement and red to the calculation. Whereas in the first image the line traces are symmetric, in the second the line traces have an antisymmetric pattern, with zero-crossing in the center of the waveguide. We find a excellent agreement between the measured and the calculated patterns. Thus, we infer that we measure the field distribution of the in-plane electric field components by using two suitably chosen orthogonal polarization in the reference branch.

Exploiting the amplitude and the phase relation between the electric field components, we reconstruct the in-plane vector field of the electric field in a single unit cell of the photonic crystal waveguide. Fig 3(a) and (b) show the experimentally and theoretically obtained vector plot of the electric field. The depicted area is $2a$ x $1a$ and the waveguide is centered around $x = 0$. The contour lines indicate the measured and calculated electric field magnitude. In a previous work Lee *et al.* measured the intensity of the electric field components in the near-field [22]. In contrast, we perform phase-sensitive measurements that allow us to determine the actual instantaneous direction of the electric field.

In the instantaneous electric vector field in Fig 3, we find a position where the electric field is at that moment zero (indicated by a black arrow). At this position the polarization state is undetermined. This is a so-called wave disclination. Such disclinations are singularities

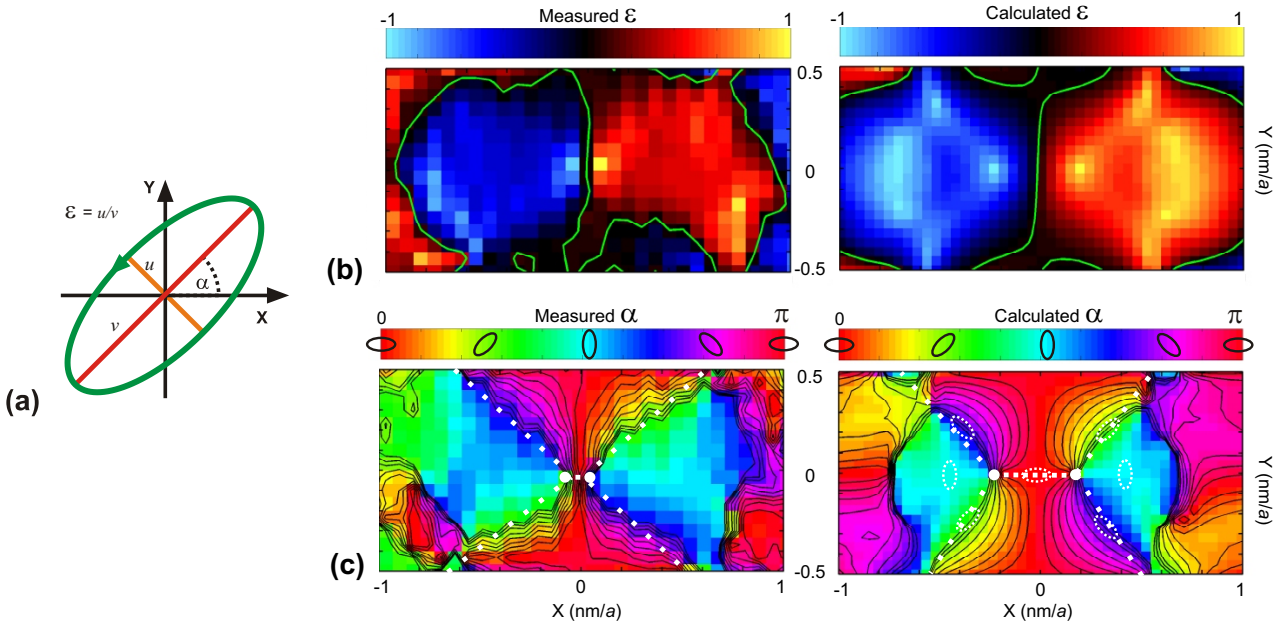

FIG. 4: (color) (a) Representation of the polarization ellipse, where v is the major semi-axis, u is the minor semi-axis of the ellipse, ε is the ellipticity and α the orientation angle. (b) Experimentally and theoretically obtained ε. Negative and positive values correspond to left- and right-handed polarization, respectively. In green lines of linear polarization (L-lines) are shown. (c) Experimentally and theoretically obtained α. The dotted ellipses indicate the orientation of the polarization and the dashed lines show the 3-fold symmetry of the system. The white dots indicate the position of C-points. The depicted area is $2a \times 1a$ (the waveguide is centered around $x = 0$).

that move as time progresses. Because around a disclination the electric field vector describes a complete circle (rotation of $\pm 2\pi$), this type of singularities are characterized with a topological charge of ± 1. The topological charge has a minus sign when the vector rotates counterclockwise after a clockwise path around a disclination and a plus sign when the vector rotates clockwise [13, 14, 29]. Around the disclination in Fig 3 the electric vectors arranged in a vortex-like arrangement. From the arrangement of the vectors around the disclination we infer that the topological charge equals $+1$. Usually, disclinations are studied in far-field transmission investigations in a plane orthogonal to the propagation direction of the light. It has been shown that the arrangement of the vectors surrounding a disclination varies as the time progresses [13, 14]. In the contrast, we investigate the polarization state in a plane parallel to the propagation direction and thus have an insight in the disclination evolution inside the sample that generates it. We observe that the topology around the disclination is in a stable vortex shape as time progresses. We attribute this to the fact that the disclination moves in the center of the waveguide, where there is a zero-crossing in E_y (see Fig 2(f)). Hence, the electric field must be parallel to the x-direction for every point along the center of the waveguide, preventing the deformation of the vortex around the dislocation.

To elucidate the polarization distribution of the light inside the photonic crystal waveguide further, we determine the ellipticity $\varepsilon = \pm \tan\{\arcsin[(\sin 2\psi)\cos\delta]/2\}$ and the orientation angle $\alpha = \arctan[(\tan 2\psi)\cos\delta]/2$ of the polarization ellipse (as illustrated in Fig 4a). The angles $\psi = \arctan(|E_y|/|E_x|)$ and $\delta = \delta_y - \delta_x$ characterize the amplitude ratio and the phase difference between the two electric field components, respectively [30]. Thus, to determine ε and α from the two field components, knowing the phase relation between them is crucial. Fig 4(b) shows the ellipticity retrieved from the measured and calculated vector field distribution of Fig 3. Negative and positive values correspond to left- and right-handed polarization, respectively. Two areas of opposite handedness are in close proximity (within 2 unit cells, or 860 nm). Fig 4(c) depicts the angle α retrieved from the calculated and measured field distribution. Note that, because $\alpha = 0$ and $\alpha = \pi$ correspond to the same polarization state, we have chosen a cyclic color map. The phase-sensitive near-field measurements and the calculations show that, in an area of the order of the square wavelength in material $[(\lambda/n)^2]$, the polarization state has an antisymmetric structure.

When the polarization is purely linear ($\varepsilon = 0$), the handedness is undetermined. This occurs along the so-called L-lines, which separate areas of opposite handedness. The above mentioned polarization disclinations must move along L-lines as time progresses [13, 29]. In

Fig 4(b) L-lines are indicated with green lines. We find a good match between measurement and calculation. The disclination observed in Fig 3 lies on the L-line in the center of the waveguide for both experiment and theory, as predicted by Nye [14].

When $\varepsilon = \pm 1$ the polarization is purely circular, which means that the orientation of the angle α is undetermined. Positions where this occurs are referred to as C-points. Around such a point the polarization ellipse describes semicircle (rotation of $\pm\pi$). Thus, these singularities are characterized by a topological charge of $\pm\frac{1}{2}$, where the sign is determined by the rotation of the direction of the ellipse around the C-point [13, 29]. In order to identify C-points, we introduce the so-called isogyres, defined as lines of equal α. These isogyres are shown in Fig 4(c) as black lines. The isogyres clearly converge on two points (white dots in Fig 4(c)) close to the center of the photonic crystal waveguide. Because by definition the isogyres are lines with one unique value of α, their intersection is possible only when α is undetermined. Thus, the intersections of the isogyres are C-points. The dashed white lines and ellipses in Fig 4b show the symmetry and ellipse orientation around the C-points, respectively. Both the C-points have topological charge $-\frac{1}{2}$ and a 3-fold type structure. This is usually referred to as a *star*. For further information about the classification of the singularities see Ref [13] and [29]. We observed that the Bloch mode propagating in a photonic crystal waveguide generates in every unit cell two circular polarization singularities in sub-wavelength proximity (200 nm according to calculation and 50 nm according to the measurements). In previous publications it has been shown that polarization singularities with the same topological charge repel each other (the so-called topological singularity screening) [17, 19, 29]. In contrast, we observe from Fig 4 that the light field generates two C-points with the same topological charge in close proximity. We attribute this to the geometrical properties of the photonic crystal waveguide that induces antisymmetric pattern of the electric field (Fig 2(f)). The topological defects distribution mirrors this antisymmetry, preventing the singularity screening effect.

In conclusion, we experimentally visualized the electric vector field of the light propagating through a photonic crystal waveguide. We observed with sub-wavelength resolution the vectorial topological defects present in the photonic crystal waveguide. We found two *star* type circular polarization singularities in sub-wavelength proximity and a disclination lying on a L-line in the center of the waveguide itself. All the measurements are in good agreement with the 3D FDTD calculations.

We wish to thank T. D. Visser helpful discussion. This work is part of the research program of the "Stichting voor Fundamenteel Onderzoek der Materie (FOM)", which is financially supported by the "Nederlandse organisatie voor Wetenschappelijk Onderzoek (NWO)". Support by the NWO (VICI grant) is gratefully acknowledged. This work is also supported by NanoNed, a nanotechnology program of the Dutch Ministry of Economic affairs.

* burresi@amolf.nl

[1] R. A. Gray, A. M. Pertsov, and J. Jalife, Nature **392**, 75 (1998).
[2] M. V. Berry, in *Proc. SPIE Vol.* (2001), vol. 4403, pp. 1–12.
[3] T. H. R. Skyrme, Proc. R. Soc. A **260**, 127 (1961).
[4] J. R. Abo-Shaeer, C. Raman, J. M. Vogels, and W. Ketterle, Science **292**, 476 (2001).
[5] K. W. Madison, F. Chevy, W. Wohlleben, and J. Dalibard, Phys. Rev. Lett. **84**, 806 (2000).
[6] M. R. Matthews, et al., Phys. Rev. Lett. **83**, 2498 (1999).
[7] A. A. Abrikosov, Sov. Phys. JETP **5**, 1174 (1957).
[8] P. Coullet, L. Gil, and J. Lega, Phys. Rev. Lett. **62**, 1619 (1989).
[9] M. Berry, Nature **403**, 21 (2000).
[10] J. F. Nye and M. V. Berry, Proc. R. Soc. A **336**, 165 (1974).
[11] N. Shvartsman and I. Freund, Phys. Rev. Lett. **72**, 1008 (1994).
[12] W. Wang, S. G. Hanson, Y. Miyamoto, and M. Takeda, Phys. Rev. Lett. **94**, 103902 (2005).
[13] J. F. Nye, *Natural focusing and fine structure of light* (Institute of Physics, Bristol, 1999).
[14] J. F. Nye, Proc. R. Soc. A (1934-1990) **387**, 105 (1983).
[15] J. F. Nye, Proc. R. Soc. A (1934-1990) **389**, 279 (1983).
[16] R. W. Schoonover and T. D. Visser, Opt. Express **14**, 5733 (2006).
[17] F. Flossmann, U. T. Schwarz, M. Maier, and M. R. Dennis, Phys. Rev. Lett. **95**, 253901 (2005).
[18] M. V. Berry, M. R. Dennis, and R. L. L. Jr, New Journal of Physics **6**, 162 (2004).
[19] R. I. Egorov, M. S. Soskin, D. A. Kessler, and I. Freund, Phys. Rev. Lett. **100**, 103901 (2008).
[20] F. Flossmann, K. O'Holleran, M. R. Dennis, and M. J. Padgett, Phys. Rev. Lett. **100**, 203902 (2008).
[21] Y. Ohdaira, T. Inoue, H. Hori, and K. Kitahara, Opt. Express **16**, 2915 (2008).
[22] K. G. Lee, et al., Nat Photon **1**, 53 (2007), see also the follow-up correspondence.
[23] Z. H. Kim and S. R. Leone, Opt. Express **16**, 1733 (2008).
[24] M. Sandtke, et al., Review of Scientific Instruments **79**, 013704 (2008).
[25] M. L. M. Balistreri, H. Gersen, J. P. Korterik, L. Kuipers, and N. F. van Hulst, Science **294**, 1080 (2001).
[26] M. L. M. Balistreri, J. P. Korterik, L. Kuipers, and N. F. van Hulst, Phys. Rev. Lett. **85**, 294 (2000).
[27] J. A. Veerman, A. M. Otter, L. Kuipers, and N. F. van Hulst, Applied Physics Letters **72**, 3115 (1998).
[28] R. J. P. Engelen, Y. Sugimoto, H. Gersen, N. Ikeda, K. Asakawa, and L. K. Kuipers, Nature Phys. **3**, 401 (2007).
[29] M. R. Dennis, Opt. Commun. **213**, 201 (2002).
[30] Born and Wolf, *Principle of optics* (Cambridge Univ. Press, Cambridge, 1999), 7th edn.